

Cite this: *J. Mater. Chem. B*, 2019,
7, 7502

Synthesis of highly selective lysosomal markers by coupling 2-(2'-hydroxyphenyl)benzothiazole (HBT) with benzothiazolium cyanine (Cy): the impact of substituents on selectivity and optical properties†

Chathura S. Abeywickrama,^a Ketil A. Bertman,^a Lucas J. McDonald,^a
Nicolas Alexander,^a Dipendra Dahal,^a Hannah J. Baumann,^a Carrie R. Salmon,^a
Chrys Wesdemiotis,^a Michael Konopka,^a Claire A. Tessier^a and Yi Pang^{*ab}

HBT-Cy **1** has been previously reported as a highly selective fluorescent probe for lysosome visualization in live cells. To further investigate the role of the structural components of HBT-Cy in lysosome selectivity, cyanine based fluorescent probe series (**2–5**) have been synthesized in good yields by connecting benzothiazolium cyanine (Cy) with 2-hydroxyphenylbenzothiazole (HBT) *via* a *meta* phenylene ring. Probes **2–5** exhibited exceptional photophysical properties including bright red-emission ($\lambda_{em} \approx 630–650$ nm), a large Stokes shift ($\Delta\lambda > 130$ nm) and high fluorescence quantum yields ($\phi_f \approx 0.1–0.5$). Probes **2**, **3**, and **5** exhibited exceptional selectivity towards cellular lysosomes in NHLF and MO3.13 cells. Our further study revealed that the phenyl benzothiazolium cyanine component (**6**) was the lysosome directing group in the HBT-Cy probe structure. The attachment of the hydroxyphenyl benzothiazole (HBT) component to the HBT-Cy probe structure has significantly improved its photophysical properties. Lysosome probes **2**, **3** and **5** exhibited excellent biocompatibility, quick staining, bright red fluorescence, and wash-free application for live cell imaging. These probes further exhibited excellent characteristics for bioimaging experiments including a non-alkalinizing nature, high biocompatibility, high photostability and long-term imaging ability (> 4 hours).

Received 7th August 2019,
Accepted 3rd October 2019

DOI: 10.1039/c9tb01672d

rsc.li/materials-b

1. Introduction

Exploring lysosome form and function is important to study severe disease conditions which occur due to lysosomal malfunction.^{1–3} Lysosomal dysfunction can lead to severe disease conditions such as lysosomal storage diseases, metabolic disorders, neurodegenerative disorders and cancer.^{1,2,4–8} Recent research has emphasized the correlation of lysosomal malfunction with possible pro-oncogenic stages.^{2,8,9} Lysosome visualization in live or fixed cell samples provides important information such as the lysosomal pH, morphology, distribution and abundance. Visualization of cellular lysosomes *via* fluorescence confocal microscopy is an advanced imaging technique currently employed for lysosome studies. A vast number of lysosome selective organic small molecule fluorescent probes have been

developed to date for various imaging applications.^{10–16} Such fluorescent probes are capable of delivering detectable fluorescence signals upon lysosomal localization. Lysosomes are membrane bound spherical organelles which contain an acidic lumen (pH $\approx 4–5$).^{1,3,17,18} The acidic environment in the lysosomal lumen is essential for the optimal activity of their degradative enzymes which are responsible for the biomacromolecule digestion process.^{5,11,18} Many lysosome-targeting probes are using the acidic environment of the lysosomal lumen in designing fluorescent probes.^{10,11,19} The most well-known strategy is to employ basic functional groups (*i.e.* amine groups) in the probe structure (*i.e.* LysoTracker[®] probes) which act as a “targeting group” towards the acidic lysosomal lumen.^{10,20} The lysosome selectivity of such probes require an acidic pH environment to operate. However, fluorescent probes with basic functional groups are well known to elevate the lysosomal pH due to their characteristic alkalinizing effect (*i.e.* LysoTracker[®] Green DND-26, LysoTracker[®] Red DND-99). Therefore, the applications of such probes are often limited to short time periods due to their inherent cytotoxicity. Alternatively, some different approaches have been employed to design spiro lactam, flavonoid and peptide-based lysosome

^a Department of Chemistry, University of Akron, Akron, Ohio 44325, USA.

E-mail: yip5@uakron.edu

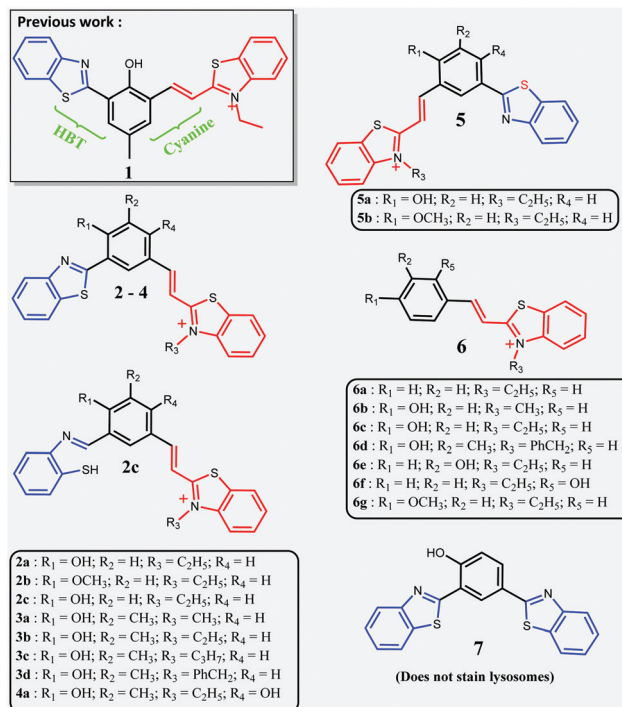
^b Maurice Morton Institute of Polymer Science, University of Akron, Akron, Ohio 44325, USA

† Electronic supplementary information (ESI) available. See DOI: 10.1039/c9tb01672d

selective fluorescent probes which do not exhibit any alkalizing effect.^{16,21–25} In an alternative approach, pyrene based lysosome directing probes have been reported recently, which are accumulated in the lysosomal membrane instead of the lysosomal lumen.¹² In addition, several ratiometric fluorescent probes have been reported for lysosome visualization.^{26–28} However, the design and synthesis of pH independent lysosome probes is still in high demand due to the recent findings of the lysosomal involvement in cancer.^{7,9,17,29–31}

Many existing commercial probes such as LysoTracker[®] Green DND-26 ($\lambda_{\text{ex}} \sim 504$ nm and $\lambda_{\text{em}} \sim 510$ nm), LysoTracker[®] Red DND-99 ($\lambda_{\text{ex}} \sim 577$ nm and $\lambda_{\text{em}} \sim 590$ nm) and LysoTracker[®] Blue DND-22 ($\lambda_{\text{ex}} \sim 380$ nm and $\lambda_{\text{em}} \sim 420$ nm) suffer from a small Stokes shift and a low signal to noise ratio (*i.e.*, acridine orange and neutral red) which limit their application in fluorescence microscopy.^{10,32} Therefore, an ideal candidate for lysosome visualization should (1) be independent of the proton uptake, (2) exhibit a large Stokes shift, (3) be highly selective, (4) provide a high signal to noise ratio, and (5) be readily excitable with the available lasers in the fluorescence microscope. In our previous work, we reported a novel lysosome selective fluorescent probe **1** by coupling 2-(2-hydroxyphenyl)benzothiazole (HBT) with benzothiazolium cyanine (Cy) *via* a *meta* phenylene ring system.¹¹ Probe **1** exhibited a remarkable selectivity towards cellular lysosomes in live cell imaging experiments. New probe **1** provided an excellent platform for designing and synthesizing a new class of lysosome selective HBT-Cy fluorescent probes. In summary, HBT-Cy based lysosome probes have several advantages over currently reported other probes including (1) structural simplicity and facile synthesis, (2) high biocompatibility, (3) long-term imaging ability, (4) non-amino group containing structure (no proton consumption within the cell), (5) lower working concentration (*i.e.*, 500 nM), (6) quick staining (7) high specificity, and (8) wash-free staining. The HBT-Cy probe skeleton also exhibits interesting photophysical characteristics due to its structural features. Remarkably a large Stokes shift ($\Delta\lambda > 130$ nm) is observed due to excited state intramolecular proton transfer (ESIPT) coupling with intra-molecular charge transfer (ICT). In addition, a large fluorescence quantum yield is observed due to the co-planar rigid geometry of the probe structure and the bright red to near infra-red (NIR) emission makes these probes ideal candidates for bioimaging applications. One of the intriguing fundamental questions is how to identify the effect of each component/substituent in a fluorophore structure on its inherent lysosome selectivity and photophysical performance.

To further investigate the role of substituents in the HBT-Cy structure, we have synthesized a library of isomeric HBT-cyanine probes of **1** (probes **2–5**) and a series of model compounds (**6–7**) with different substituents and connectivity (Schemes 1 and 2). The isomeric probe versions **2–5** were synthesized by altering the substituents and connectivity across the HBT-Cy fluorophore skeleton. Probes **2**, **3** and **5** exhibited exceptional lysosome selectivity in normal human lung fibroblast (NHLF) and MO3.13 progenitor oligodendrocyte cell line under wash-free conditions. In this work we further discuss the



Scheme 1 Structures of the lysosome selective probes (**2–6**).

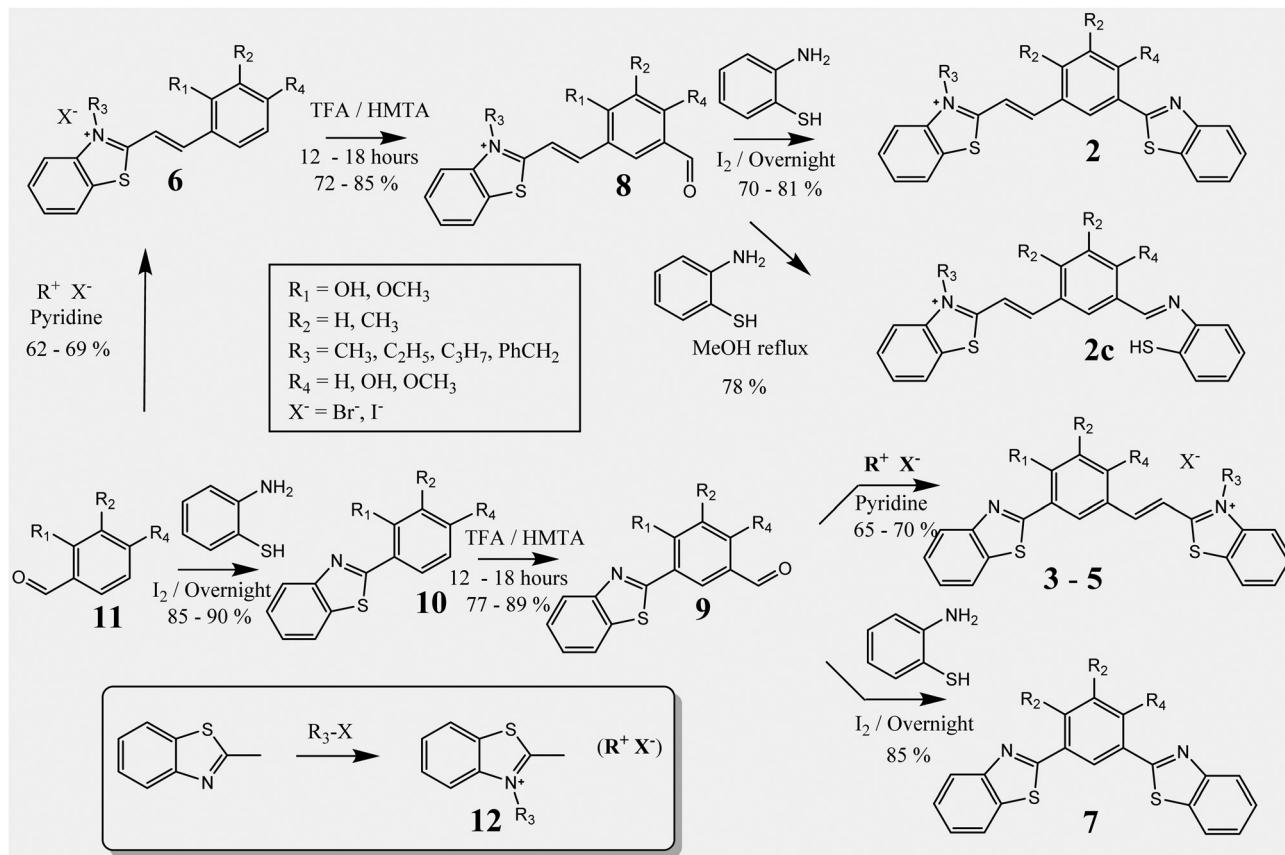
importance of the structural features in the observed lysosome selectivity and optical properties by considering the role of each components in the HBT-Cy structure.

2. Materials and methods

All solvents and reagents were used as received without further purification unless specified otherwise. Reactions were performed under standard atmospheric conditions in oven-dried glassware. All molecular biology grade reagents for cell culture and fluorescence confocal microscopy were purchased from Fisher Scientific. UV-Vis spectra were obtained using a Hewlett Packard-8453 diode array spectrophotometer at 25 °C. Fluorescence spectra were measured using a HORIBA Fluoromax-4 spectrofluorometer. ¹H NMR spectra were obtained using a Varian 300 MHz spectrometer in deuterated dimethyl sulfoxide (d-DMSO) or chloroform (CDCl₃) solvents. Fluorescence confocal laser microscopy imaging was performed using a Nikon A1 system with a 60× or 100× oil objective.

2.1 Synthesis

2.1.1 General procedure for synthesis of 2a, 2b and 7. In a flask, 1 mmol of the corresponding aldehyde (**8–9**) was dissolved in 20 mL of methanol. Then, the corresponding 2-aminothiophenol (1.2 mmol) was added and the solution was stirred at room temperature for 5 minutes. Then I₂ (10% by the aldehyde mole) was added and the resulting solution was stirred at room temperature for 12 hours. After completion of the reaction, the resulting product was collected by vacuum filtration and washed with cold methanol (3 × 10 mL) 3 times.



Scheme 2 Synthesis of probes 2–7.

The desired product (**2a**, **2b** and **7**) was collected using a Buchner funnel (70–85%).

(E)-2-(3-(Benzo[*d*]thiazol-2-yl)-4-hydroxystyryl)-3-ethylbenzo[*d*]thiazol-3-ium iodide (**2a**). **2a** was obtained as a dark green powder with 66% yield. $^1\text{H NMR}$ (300 MHz in DMSO) δ 11.18 (s, 1H), 8.36 (d, $J = 8.01$ Hz, 1H), 8.22 (m, 2H), 8.02 (d, $J = 11.1$ Hz, 1H), 7.83 (t, $J = 7.8$ Hz, 2H), 7.73 (m, 1H), 6.96 (t, $J = 8.5$ Hz, 2H), 6.80 (m, 2H), 6.53 (d, $J = 7.4$ Hz, 2H), 4.90 (q, $J = 6.6$ Hz, 2H), and 1.41 (t, $J = 6.4$ Hz, 3H). HRMS (ESI) found (m/z) for $[\text{C}_{24}\text{H}_{19}\text{N}_2\text{OS}_2]^+$ 415.0952, 416.1301 and 417.1438. Calculated (m/z) for $[\text{C}_{24}\text{H}_{19}\text{N}_2\text{OS}_2]^+$ 415.0939, 416.0939 and 417.0939.

(E)-2-(3-(Benzo[*d*]thiazol-2-yl)-4-methoxystyryl)-3-ethylbenzo[*d*]thiazol-3-ium iodide (**2b**). **2b** was obtained as a dark orange powder with 70% yield. $^1\text{H NMR}$ (300 MHz in DMSO) δ 8.44 (d, $J = 8.1$ Hz, 1H), 8.26 (dt, $J = 15.6, 8.1$ Hz, 2H), 8.03 (s, 1H), 7.80 (m, 3H), 7.29 (t, $J = 10.1$ Hz, 1H), 6.95 (m, 3H), 6.77 (m, 2H), 4.93 (q, $J = 6.8$ Hz, 2H), 3.97 (s, 3H), and 1.46 (t, $J = 6.5$ Hz, 3H). HRMS (ESI) found (m/z) for $[\text{C}_{25}\text{H}_{21}\text{N}_2\text{OS}_2]^+$ 429.1048, 430.1341 and 431.1341. Calculated (m/z) for $[\text{C}_{25}\text{H}_{21}\text{N}_2\text{OS}_2]^+$ 429.1095, 430.1095 and 431.1095.

2.1.2 Synthesis of 2c. In a flask, 1 mmol of the corresponding aldehyde (**8**) was dissolved in 20 mL of methanol. Then, the corresponding 2-aminothiophenol (1.1 mmol) was added and the solution was refluxed for 3 hours. After completion of the reaction, 10 mL of ethyl acetate was added to the mixture and

the resulting product was collected by vacuum filtration and washed with cold ethyl acetate (3×10 mL) 3 times. The desired product (**2c**) was collected using a Buchner funnel (78% yield).

3-Ethyl-2-((*E*)-4-hydroxy-3-((*E*)-((2-mercaptophenyl)imino)methyl)styryl)benzo[*d*]thiazol-3-ium iodide (**2c**). **2c** was obtained as a dark grey powder with 77% yield. $^1\text{H NMR}$ (300 MHz in DMSO) δ 12.56 (s, 1H), 8.85 (d, $J = 5.5$ Hz, 1H), 8.46 (m, 2H), 8.30 (s, 1H), 8.19 (t, $J = 6.7$ Hz, 1H), 8.11 (t, $J = 6.8$ Hz, 1H), 7.86 (m, 3H), 7.55 (dq, $J = 29.6, 7.0$ Hz, 2H), 7.23 (m, 1H), 7.01 (dq, $J = 21.6, 6.7$ Hz, 1H), 6.71 (t, $J = 7.0$ Hz, 1H), 6.41 (q, $J = 7.1$ Hz, 1H), 5.44 (s, 1H), 4.95 (q, $J = 6.8$ Hz, 2H), and 1.47 (t, $J = 6.7$ Hz, 3H). HRMS (ESI) found (m/z) for $[\text{C}_{24}\text{H}_{21}\text{N}_2\text{OS}_2]^+$ 417.1051, 418.1350 and 419.1360. Calculated (m/z) for $[\text{C}_{24}\text{H}_{21}\text{N}_2\text{OS}_2]^+$ 417.1095, 418.1095 and 419.1095.

2.1.3 General procedure for synthesis of 3–5. In a flask, 1.1 mmol of the corresponding aldehyde (**8–9**) was dissolved in 25 mL of methanol. Then, the corresponding 2-methylbenzothiazolium salt **12** (R^+X^- ; 1.0 mmol) was added and the solution was stirred at room temperature for 10 minutes. Following the addition of pyridine (0.25 mL), the resulting solution was heated up and stirred at 65 °C for 12 hours. After completion of the reaction, the reaction mixture was cooled down to room temperature and concentrated under vacuum. To the resulting dark red crude, ethyl acetate (10 mL) was added, and the product was precipitated as a dark colored solid in the bottom

of the flask. After the solution was allowed to settle for 15 minutes, the resulting solid was collected by vacuum filtration and washed with ethyl acetate (3×10 mL) 3 times. The desired product (**3–5**) was collected using a Buchner funnel (65–85% yield).

(*E*)-2-(3-(Benzo[d]thiazol-2-yl)-4-hydroxy-5-methylstyryl)-3-methylbenzo[d]thiazol-3-ium iodide (**3a**). **3a** was obtained as a dark red powder with 69% yield. ^1H NMR (300 MHz in DMSO) δ 13.16 (s, 1H) 8.43 (m, 1H), 8.33 (d, $J = 4.2$ Hz, 1H), 8.22 (m, 3H), 8.11 (dd, $J = 8.1, 4.2$ Hz, 1H), 7.94 (d, $J = 4.2$ Hz, 1H), 7.88 (m, 1H), 7.86 (dd, $J = 7.7, 4.1$ Hz, 1H), 7.56 (m, 1H), 7.54 (dd, $J = 7.8, 4.1$ Hz, 1H), 4.35 (s, 3H), and 2.36 (s, 3H). HRMS (ESI) found (m/z) for $[\text{C}_{24}\text{H}_{19}\text{N}_2\text{OS}_2]^+$ 415.0940, 416.1288 and 417.1425. Calculated (m/z) for $[\text{C}_{24}\text{H}_{19}\text{N}_2\text{OS}_2]^+$ 415.0939, 416.0939 and 417.0939.

(*E*)-2-(3-(Benzo[d]thiazol-2-yl)-4-hydroxy-5-methylstyryl)-3-ethylbenzo[d]thiazol-3-ium iodide (**3b**). **3b** was obtained as a dark brown powder with 70% yield. ^1H NMR (300 MHz in DMSO) δ 13.17 (s, 1H) 8.44 (m, 2H), 8.39 (q, $J = 9.0, 8.0$ Hz, 5H), 8.12 (d, $J = 8.0$ Hz, 1H), 7.90 (m, 2H), 7.79 (d, $J = 7.6$ Hz, 1H), 7.60 (d, $J = 7.6$ Hz, 1H), 7.52 (d, $J = 7.6$ Hz, 1H), 4.98 (q, $J = 6.9$ Hz, 2H), 2.39 (s, 3H), and 1.47 (t, $J = 6.5$ Hz, 3H). HRMS (ESI) found (m/z) for $[\text{C}_{25}\text{H}_{21}\text{N}_2\text{OS}_2]^+$ 429.1088, 430.1457 and 431.1533. Calculated (m/z) for $[\text{C}_{25}\text{H}_{21}\text{N}_2\text{OS}_2]^+$ 429.1095, 430.1095 and 431.1095.

(*E*)-2-(3-(Benzo[d]thiazol-2-yl)-4-hydroxy-5-methylstyryl)-3-propylbenzo[d]thiazol-3-ium iodide (**3c**). **3c** was obtained as a dark green powder with 67% yield. ^1H NMR (300 MHz in DMSO) δ 13.16 (s, 1H) 8.42 (m, 3H), 8.30 (m, 3H), 8.12 (d, $J = 7.4$ Hz, 1H), 7.83 (m, 3H), 7.53 (m, 2H) 4.92 (t, $J = 6.4$ Hz, 2H), 2.39 (s, 3H), 1.91 (m, 2H) and 1.00 (t, $J = 6.2$ Hz, 3H). HRMS (ESI) found (m/z) for $[\text{C}_{26}\text{H}_{23}\text{N}_2\text{OS}_2]^+$ 443.1246, 444.1473 and 445.1711. Calculated (m/z) for $[\text{C}_{26}\text{H}_{23}\text{N}_2\text{OS}_2]^+$ 443.1252, 444.1252 and 445.1252.

(*E*)-2-(3-(Benzo[d]thiazol-2-yl)-4-hydroxy-5-methylstyryl)-3-benzylbenzo[d]thiazol-3-ium bromide (**3d**). **3d** was obtained as a dark brown powder with 68% yield. ^1H NMR (300 MHz in DMSO) δ 8.44 (m, 3H), 8.20 (m, 6H), 8.22 (d, $J = 7.7$ Hz, 3H), 7.75 (d, $J = 7.8$ Hz, 2H), 7.55 (m, 3H), 6.25 (s, 2H), and 2.37 (s, 3H). HRMS (ESI) found (m/z) for $[\text{C}_{30}\text{H}_{23}\text{N}_2\text{OS}_2]^+$ 491.1244, 492.1439 and 493.1726. Calculated (m/z) for $[\text{C}_{30}\text{H}_{23}\text{N}_2\text{OS}_2]^+$ 491.1252, 492.1252 and 493.1252.

(*E*)-2-(5-(Benzo[d]thiazol-2-yl)-2,4-dihydroxy-3-methylstyryl)-3-ethylbenzo[d]thiazol-3-ium iodide (**4a**). **4a** was obtained as a dark grey powder with 65% yield. ^1H NMR (300 MHz in DMSO) δ 8.41 (d, $J = 7.1$ Hz, 1H), 8.36 (d, $J = 7.4$ Hz, 2H), 8.19 (m, 2H), 8.06 (d, $J = 7.6$ Hz, 1H), 7.99 (dd, $J = 14.9, 4.8$ Hz, 1H), 7.50 (dd, $J = 19.7, 4.9$ Hz, 2H), 4.92 (q, $J = 6.9$ Hz, 2H), 2.22 (s, 3H), and 1.51 (t, $J = 6.4$ Hz, 3H). HRMS (ESI) found (m/z) for $[\text{C}_{25}\text{H}_{21}\text{N}_2\text{O}_2\text{S}_2]^+$ 445.1091, 446.1263 and 447.1369. Calculated (m/z) for $[\text{C}_{25}\text{H}_{21}\text{N}_2\text{O}_2\text{S}_2]^+$ 445.1045, 446.1045 and 447.1045.

(*E*)-2-(5-(Benzo[d]thiazol-2-yl)-2-hydroxystyryl)-3-ethylbenzo[d]thiazol-3-ium iodide (**5a**). **5a** was obtained as a dark brown powder with 81% yield. ^1H NMR (300 MHz in DMSO) δ 11.76 (s, 1H) 8.67 (d, $J = 7.4$ Hz, 1H), 8.44 (d, $J = 7.6$ Hz, 2H), 8.34 (d, $J = 7.6$ Hz, 1H), 8.16 (m, 4H), 7.82 (dd, $J = 16.3, 4.2$ Hz, 2H),

7.51 (m, 2H), 7.21 (d, $J = 7.5$ Hz, 1H), 4.98 (q, $J = 6.2$ Hz, 2H), and 1.50 (t, $J = 6.0$ Hz, 3H). HRMS (ESI) found (m/z) for $[\text{C}_{24}\text{H}_{19}\text{N}_2\text{OS}_2]^+$ 415.0969, 416.1243 and 417.1304. Calculated (m/z) for $[\text{C}_{24}\text{H}_{19}\text{N}_2\text{OS}_2]^+$ 415.0939, 416.0939 and 417.0939.

(*E*)-2-(5-(Benzo[d]thiazol-2-yl)-2-methoxystyryl)-3-ethylbenzo[d]thiazol-3-ium iodide (**5b**). **5b** was obtained as a dark yellow powder with 70% yield. ^1H NMR (300 MHz in DMSO) δ 8.82 (d, $J = 7.6$ Hz, 1H), 8.47 (d, $J = 7.4$ Hz, 1H), 8.33 (m, 2H), 8.23 (d, $J = 7.3$ Hz, 1H), 8.10 (m, 3H), 7.83 (dd, $J = 17.4, 4.8$ Hz, 2H), 7.15 (d, $J = 7.5$ Hz, 2H), 5.00 (q, $J = 6.7$ Hz, 2H), 3.86 (s, 3H), and 1.50 (t, $J = 6.5$ Hz, 3H). HRMS (ESI) found (m/z) for $[\text{C}_{25}\text{H}_{21}\text{N}_2\text{OS}_2]^+$ 429.1093, 430.1233 and 431.1234. Calculated (m/z) for $[\text{C}_{25}\text{H}_{21}\text{N}_2\text{OS}_2]^+$ 429.1095, 430.1095 and 431.1095.

2.1.4 General procedure for synthesis of 6. In a flask, 1.1 mmol of the corresponding aldehyde (**11**) was dissolved in 20 mL of methanol. Then, the corresponding 2-methyl benzo-thiazolium salt **12** (R^+X^- ; 1.0 mmol) was added and the solution was stirred at room temperature for 10 minutes. Following the addition of pyridine (0.5 mL), the resulting solution was heated up and stirred at 65 °C for 18 hours. After completion of the reaction, the reaction mixture was cooled down to room temperature and concentrated under vacuum. To the resulting dark red crude, ethyl acetate (10 mL) was added, and the product was precipitated as a colored solid in the bottom of the flask. After the solution was allowed to settle for 15 minutes, the resulting solid was collected by vacuum filtration and washed with ethyl acetate (3×10 mL) 3 times. The desired product (**6**) was collected using a Buchner funnel (62–69% yield).

(*E*)-3-Ethyl-2-styrylbenzo[d]thiazol-3-ium iodide (**6a**). **6a** was obtained as a yellow powder with 62% yield. ^1H NMR (300 MHz in DMSO) δ 8.44 (d, $J = 7.0$ Hz, 1H), 8.22 (dd, $J = 17.9, 4.7$ Hz, 2H), 8.07 (m, 3H), 7.86 (m, 2H), 7.56 (m, 3H), 4.97 (q, $J = 6.8$ Hz, 2H), and 1.47 (t, $J = 6.5$ Hz, 3H). HRMS (ESI) found (m/z) for $[\text{C}_{17}\text{H}_{16}\text{NS}^+]$ 266.1003, 267.1215 and 268.1316. Calculated (m/z) for $[\text{C}_{17}\text{H}_{16}\text{NS}^+]$ 266.1003, 267.1003 and 268.1003.

(*E*)-2-(4-Hydroxystyryl)-3-methylbenzo[d]thiazol-3-ium iodide (**6b**). **6b** was obtained as a dark red powder with 65% yield. ^1H NMR (300 MHz in DMSO) δ 10.56 (s, 1H), 8.38 (d, $J = 7.3$ Hz, 1H), 8.17 (m, 2H), 7.92 (d, $J = 7.1$ Hz, 2H), 7.81 (d, $J = 7.4$ Hz, 1H), 7.76 (m, 2H), 6.94 (d, $J = 6.8$ Hz, 2H), and 4.26 (s, 3H). HRMS (ESI) found (m/z) for $[\text{C}_{16}\text{H}_{14}\text{NOS}^+]$ 268.0782, 269.1091 and 270.1238. Calculated (m/z) for $[\text{C}_{16}\text{H}_{14}\text{NOS}^+]$ 268.0796, 269.0796 and 270.0796.

(*E*)-3-Ethyl-2-(4-hydroxystyryl)benzo[d]thiazol-3-ium iodide (**6c**). **6c** was obtained as dark yellow powder with 69% yield. ^1H NMR (300 MHz in DMSO) δ 10.58 (s, 1H), δ 8.37 (d, $J = 7.4$ Hz, 1H), 8.27 (d, $J = 7.2$ Hz, 1H), 8.12 (d, $J = 7.4$ Hz, 1H), 7.95 (d, $J = 7.1$ Hz, 2H), 7.81 (d, $J = 6.9$ Hz, 1H), 7.77 (m, 3H), 6.94 (d, $J = 7.7$ Hz, 2H), 4.89 (q, $J = 6.6$ Hz, 2H), and 1.45 (t, $J = 6.7$ Hz, 3H). HRMS (ESI) found (m/z) for $[\text{C}_{17}\text{H}_{16}\text{NOS}^+]$ 282.1014, 283.1280 and 284.1192. Calculated (m/z) for $[\text{C}_{17}\text{H}_{16}\text{NOS}^+]$ 282.0953, 283.0953 and 284.0953.

(*E*)-3-Benzyl-2-(4-hydroxystyryl)benzo[d]thiazol-3-ium bromide (**6d**). **6d** was obtained as an orange powder with 67% yield. ^1H NMR (300 MHz in DMSO) δ 10.66 (s, 1H), 8.41 (d, $J = 7.6$ Hz, 1H),

8.25 (d, $J = 7.3$ Hz, 1H), 8.11 (d, $J = 7.6$ Hz, 1H), 7.92 (m, 3H), 7.79 (m, 2H), 7.33 (m, 5H), 6.92 (d, $J = 7.9$ Hz, 2H), and 6.22 (s, 2H). HRMS (ESI) found (m/z) for $[C_{22}H_{18}NOS^+]$ 344.1088, 345.1330 and 346.1451. Calculated (m/z) for $[C_{22}H_{18}NOS^+]$ 344.1109, 345.1109 and 346.1109.

(*E*)-3-Ethyl-2-(3-hydroxystyryl)benzo[d]thiazol-3-ium iodide (**6e**). **6e** was obtained as a yellow-green powder with 68% yield. 1H NMR (300 MHz in DMSO) δ 9.80 (s, 1H), 8.43 (d, $J = 7.4$ Hz, 1H), 8.32 (d, $J = 7.1$ Hz, 1H), 8.13 (d, $J = 7.6$ Hz, 1H), 7.86 (m, 3H), 7.44 (m, 3H), 7.01 (d, $J = 7.2$ Hz, 2H), 4.96 (q, $J = 6.9$ Hz, 2H), and 1.47 (t, 6.3 Hz, 3H). HRMS (ESI) found (m/z) for $[C_{17}H_{16}NOS^+]$ 282.0912, 283.1301 and 284.1337. Calculated (m/z) for $[C_{17}H_{16}NOS^+]$ 282.0953, 283.0953 and 284.0953.

(*E*)-3-Ethyl-2-(2-hydroxystyryl)benzo[d]thiazol-3-ium iodide (**6f**). **6f** was obtained as a green powder with 63% yield. 1H NMR (300 MHz in DMSO) δ 10.85 (s, 1H), 8.40 (d, $J = 7.7$ Hz, 1H), 8.28 (d, $J = 7.3$ Hz, 2H), 8.01 (dd, $J = 17.5, 4.5$ Hz, 2H), 7.80 (m, 2H), 7.39 (m, 1H), 6.98 (m, 2H), 4.92 (q, $J = 6.4$ Hz, 2H), and 1.45 (t, $J = 6.1$ Hz, 3H). HRMS (ESI) found (m/z) for $[C_{17}H_{16}NOS^+]$ 282.0912, 283.1239 and 284.1275. Calculated (m/z) for $[C_{17}H_{16}NOS^+]$ 282.0953, 283.0953 and 284.0953.

(*E*)-3-Ethyl-2-(4-methoxystyryl)benzo[d]thiazol-3-ium iodide (**6g**). **6g** was obtained as a yellow powder with 67% yield. 1H NMR (300 MHz in DMSO) δ 8.42 (d, $J = 7.5$ Hz, 1H), 8.24 (d, $J = 7.2$ Hz, 1H), 8.19 (d, $J = 7.5$ Hz, 1H), 8.06 (d, $J = 7.6$ Hz, 2H), 7.86 (m, 2H), 7.77 (d, $J = 7.3$ Hz, 1H), 7.12 (d, $J = 7.4$ Hz, 2H), 4.95 (q, $J = 7.9$ Hz, 2H), 3.88 (s, 3H), and 1.45 (t, $J = 6.4$ Hz, 3H). HRMS (ESI) found (m/z) for $[C_{18}H_{18}NOS^+]$ 296.1098, 297.1170 and 298.1134. Calculated (m/z) for $[C_{18}H_{18}NOS^+]$ 296.1109, 297.1109 and 298.1109.

2.1.5 Synthesis of 7. In a flask, 1 mmol of the corresponding aldehyde (**9**) was dissolved in 20 mL of methanol. Then, the corresponding 2-aminothiophenol (1.2 mmol) was added and the solution was stirred at room temperature for 5 minutes. Then I_2 (0.1 mmol) was added and the resulting solution was stirred at room temperature for 10 hours. After completion of the reaction, the resulting product was deposited on the bottom of the flask. Then the product was collected by vacuum filtration and washed with cold methanol (3×10 mL) 3 times. The desired product (**9**) was collected using a Buchner funnel (85% yield).

2,4-Bis(benzo[d]thiazol-2-yl)phenol (**7**). **7** was obtained as a light-yellow powder with 81% yield. 1H NMR (300 MHz in DMSO) δ 12.16 (s, 1H), 9.05 (d, $J = 7.8$ Hz, 1H), 8.15 (m, 3H), 8.08 (d, $J = 7.6$ Hz, 2H), 7.54 (d, $J = 7.7$ Hz, 2H), 7.47 (d, $J = 7.6$ Hz, 2H), and 7.24 (d, $J = 7.4$ Hz, 1H). HRMS (ESI) found (m/z) for $[C_{20}H_{13}N_2OS_2^+]$ 361.0474, 362.0616 and 363.0632. Calculated (m/z) for $[C_{20}H_{13}N_2OS_2^+]$ 361.0469, 362.0469 and 363.0469.

2.1.6 General procedure for synthesis of 8. In a flask, 1 mmol of the corresponding benzothiazolium salt (**6**) and HMTA (1.2 mmol) were dissolved in 10 mL of trifluoroacetic acid. Then, the mixture was refluxed overnight (~ 12 hours). After completion of the reaction, the resulting reaction mixture was cooled down to 0 °C and neutralized with dilute NaOH.

Then the solid deposited on the bottom of the flask was collected by vacuum filtration and washed with ice cold ethyl acetate (15 mL). The desired product (**8**) was collected using a Buchner funnel (72% 85% yield).

(*E*)-3-Ethyl-2-(3-formyl-4-hydroxystyryl)benzo[d]thiazol-3-ium iodide (**8a**). **8a** was obtained as a red powder with 85% yield. 1H NMR (300 MHz in DMSO) δ 11.89 (s, 1H), 10.35 (s, 1H), 8.41 (d, $J = 8.0$ Hz, 1H), 8.25 (m, 3H), 7.96 (s, 1H), 7.83 (m, 2H), 7.16 (d, $J = 7.6$ Hz, 1H), 4.96 (q, $J = 6.6$ Hz, 2H), and 1.43 (t, $J = 6.4$ Hz, 3H). HRMS (ESI) found (m/z) for $[C_{18}H_{16}NO_2S^+]$ 310.0891, 311.1134 and 312.1134. Calculated (m/z) for $[C_{18}H_{16}NO_2S^+]$ 310.0902, 311.0902 and 312.0902.

(*E*)-3-Ethyl-2-(3-formyl-4-methoxystyryl)benzo[d]thiazol-3-ium iodide (**8b**). **8b** was obtained as an orange powder. 1H NMR (300 MHz in DMSO) δ 10.41 (s, 1H), 8.42 (d, $J = 7.8$ Hz, 2H), 8.30 (t, $J = 7.7$ Hz, 2H), 8.01 (d, $J = 7.4$ Hz, 1H), 7.86 (m, 3H), 7.42 (d, $J = 7.4$ Hz, 2H), 4.98 (q, $J = 6.6$ Hz, 2H), 4.06 (s, 3H), and 1.45 (t, $J = 6.3$ Hz, 3H). HRMS (ESI) found (m/z) for $[C_{19}H_{18}NO_2S^+]$ 324.1090, 325.1364 and 326.1388. Calculated (m/z) for $[C_{19}H_{18}NO_2S^+]$ 324.1058, 325.1058 and 326.1058.

2.2 Fluorescence quantum yield calculation

The fluorescence quantum yields (ϕ_f) for compounds were calculated by using quinine sulfate or Rhodamine 6G (Sigma) as the standard. The following equation was used for the calculation:

$$(\phi_f)_{\text{sample}} = \phi_{\text{ref}} \times (\text{Abs}_{\text{ref}}/\text{Abs}_{\text{sample}}) \times (I_{\text{sample}}/I_{\text{ref}}) \times (\eta_{\text{sample}})^2/(\eta_{\text{ref}})^2$$

where Abs is the absorbance of the sample, I is the integrated fluorescence emission intensity and η is the refractive index of the solvent.

2.3 Live cell imaging

Fluorescence confocal microscopy imaging was performed using a Nikon A1 confocal system with a 60 \times and 100 \times oil objective with a numerical aperture of 1.45 and a refractive index of 1.5. The imaging temperature was maintained at 37 °C at all time. The excitation wavelengths used for our dyes were 405 nm and 561 nm. Standard DAPI, FITC, mCherry and Cy5 emission filters were used. All imaging was done using an Okolab Bold Cage Incubator or at 37 °C, and the images were processed using NIS Elements or ImageJ Pro (NIH) imaging software. The overlap coefficients were calculated by using the ImageJ (NIH) software ($n > 30$). Commercial LysoTracker[®] Green DND-26 and MitoTracker[®] Green-FM probes were excited using a 488 nm laser line and emission was collected in the range of 495–550 nm. Commercial LysoTracker[®] Red DND-99 was excited with a 561 nm laser line and emission was collected in the 570 nm to 700 nm range. The probes were excited with a 405 or 561 nm laser line and emissions were collected according to the characteristic emission.

Note: Co-localization experiments were conducted with laser lines in multiple tracks cautiously to avoid any possible background interferences. No background fluorescence signal was obtained for LysoTracker[®] Green with a 405 nm laser line.

2.4 Cell culturing and staining

For imaging experiments, probe stock solutions were prepared in DMSO and the total DMSO% in imaging solutions was maintained below 0.1% (v/v). NHLFs (normal human lung fibroblasts) and MO3.13 cells (progenitor oligodendrocytes) were plated on a Mat Tek 35 mm dish with glass bottom at a density of 1×10^5 cells per plate in DMEM enriched with 10% fetal bovine serum (Gibco) and 1% penicillin/streptomycin. The cells were incubated overnight at 37 °C and in 5% CO₂. Subsequent to incubation, the cells were washed with 1 × PBS and treated with 0.5 μM probe (2–6) in Invitrogen™ Molecular Probes™ Live Cell Imaging Solution for 30 min. After treatment, the cells were washed once for 1 minute with 1 × PBS. Invitrogen™ Molecular Probes™ Live Cell Imaging Solution was added to the cells for imaging. Lyotracker® stock solution was made with DMSO and the total DMSO levels were maintained in the media were below 0.25% (v/v%). All cells were maintained in a 5% CO₂ humidified atmosphere at 37 °C.

2.5 Cell viability assay

The viability of NHLF cells following treatment with probes (2–5) was evaluated using Biotium MTT assay. NHLFs were plated in a 96 well plate at a density of 7.3×10^4 cells per mL in DMEM with 10% FBS and 1% penicillin/streptomycin and allowed to adhere overnight at 37 °C with 5% CO₂. Probes, 0.14–70 μM, or vehicle control, 0.5% DMSO, were dissolved in DMEM with 10% FBS and 1% penicillin/streptomycin. Each treatment concentration was applied in triplicate, with the exception of the vehicle control being applied to 12 wells and incubated for 24 hours. After 24 hours, the media and the treated probes were aspirated and replaced with DMEM with 10% FBS and 1% penicillin/streptomycin containing 0.1 mg mL⁻¹ MTT and incubated for 3.5 hours at 37 °C. The plates were centrifuged at 1000 × g for 10 minutes, after which the medium was carefully aspirated and replaced with MTT solvent, prepared

according to the MTT manufacturer's instruction. From this point, the plates were protected from light and placed on a shaker for 15 minutes. The absorbance values were read at 570 nm with a reference at 630 nm. The percent viability was determined using the following equation ($(treatment\ absorbance - blank)/(average\ vehicle\ control\ absorbance - blank) \times 100$). The dose response curves and statistics were generated using the GraphPad Prism 5 software.

3. Results and discussion

3.1 Synthesis

The desired products 2–6 were synthesized according to Scheme 2. Products 2–6 were further purified by precipitation in absolute ethyl acetate. All products were obtained in good yields (65–90%) and characterized by ¹H NMR spectroscopy and high-resolution mass spectrometry (ESI,† Fig. S2 and S3).

3.2 Spectroscopic properties

The spectroscopic properties of probes 2–6 were studied in different solvents and reported in Table 1 and the ESI,† Fig. S4. Probes 6a to 6g exhibited a significantly weaker emission in all solvents (Table 1) in comparison with probes 2–5. The observed low fluorescence quantum yield in 6 ($\phi_f \approx 0.001$ –0.007) can be explained by considering the possible high degree of non-radiative relaxation in skeleton 6. In comparison to probe 6a ($\lambda_{em} \approx 385$ nm and $\lambda_{em} \approx 475$ nm in DCM) the attachment of a moderate donor group (*i.e.*, OH) *via* the *para* position of the skeleton (6b–6d) could significantly enhance the ICT process in the molecule which leads to a noticeable bathochromic shift in the optical spectra of the probes ($\lambda_{ex} \approx 450$ nm and $\lambda_{em} \approx 530$ nm in DCM). In addition, the attachment of the donor group (–OH) *via* the *ortho* position (6f) also exhibited a similar effect. Probe 6e with *meta* hydroxy connectivity to the benzothiazolium moiety did not exhibit a noticeable bathochromic

Table 1 Spectroscopic properties of probes 2–7

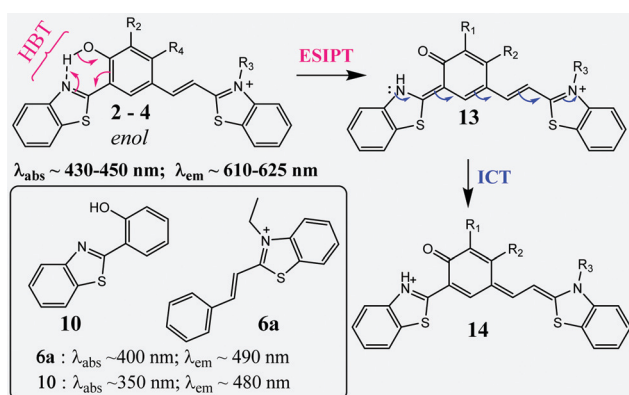
| Entry | Spectroscopic properties in different solvents | | | | | | | | | | | | |
|-------|--|-------------------------------------|-------------------------|-------------------------------------|-------------------------|-------------------------------------|-------------------------|-------------------------------------|-------------------------|-------------------------------------|--|--|--|
| | Benzene | | DCM | | DMSO | | EtOH | | Water | | ϵ (M ⁻¹ cm ⁻¹) ^(DCM) | $\Delta\lambda$ (cm ⁻¹) (DCM) | |
| | λ_{abs} (nm) | λ_{em} (nm) (ϕ_f) | λ_{abs} (nm) | λ_{em} (nm) (ϕ_f) | λ_{abs} (nm) | λ_{em} (nm) (ϕ_f) | λ_{abs} (nm) | λ_{em} (nm) (ϕ_f) | λ_{abs} (nm) | λ_{em} (nm) (ϕ_f) | | | |
| 2a | 415 | 605 (0.0016) | 440 | 608 (0.17) | 418 | 609 (0.41) | 433 | 614 (0.24) | 405 | 591 (0.0071) | 33 624 | 6280 | |
| 2b | 423 | 495 (0.0020) | 429 | 526 (0.06) | 407 | 528 (0.12) | 414 | 515 (0.08) | 402 | 532 (0.0032) | 22 176 | 4298 | |
| 3a | 420 | 605 (0.0014) | 450 | 618 (0.14) | 413 | 626 (0.45) | 426 | 623 (0.28) | 401 | 590 (0.0015) | 40 346 | 6041 | |
| 3b | 421 | 608 (0.0024) | 449 | 614 (0.13) | 414 | 625 (0.47) | 427 | 620 (0.34) | 403 | 599 (0.0027) | 42 269 | 5988 | |
| 3c | 422 | 612 (0.0022) | 449 | 614 (0.13) | 415 | 627 (0.42) | 429 | 619 (0.31) | 405 | 605 (0.0022) | 40 952 | 5985 | |
| 3d | 428 | 610 (0.0018) | 456 | 626 (0.15) | 420 | 634 (0.52) | 435 | 631 (0.41) | 397 | 600 (0.0031) | 45 613 | 5956 | |
| 4a | 449 | 603 (0.0018) | 470 | 607 (0.19) | 450 | 641 (0.62) | 458 | 635 (0.27) | 430 | 620 (0.0032) | 43 438 | 4802 | |
| 5a | 442 | 588 (0.0015) | 455 | 612 (0.110) | 428 | 641 (0.310) | 431 | 617 (0.244) | 424 | 615 (0.0030) | 36 193 | 5638 | |
| 5b | 439 | 581 (0.0013) | 456 | 595 (0.071) | 423 | 600 (0.085) | 430 | 588 (0.036) | 408 | 612 (0.0036) | 34 416 | 5123 | |
| 6a | 380 | 438 (0.0001) | 387 | 475 (0.0021) | 377 | 471 (0.0040) | 376 | 464 (0.0015) | 370 | 452 (0.0006) | 32 276 | 4787 | |
| 6b | 428 | 505 (0.0021) | 447 | 527 (0.0038) | 424 | 526 (0.0058) | 429 | 511 (0.0032) | 406 | 515 (0.0003) | 45 486 | 3397 | |
| 6c | 450 | 523 (0.0002) | 452 | 532 (0.0051) | 426 | 528 (0.0071) | 430 | 515 (0.0042) | 405 | 514 (0.0002) | 42 188 | 3327 | |
| 6d | 451 | 504 (0.0003) | 460 | 536 (0.0061) | 431 | 531 (0.0141) | 438 | 518 (0.0052) | 415 | 520 (0.0004) | 54 886 | 3083 | |
| 6e | 391 | 500 (0.0006) | 396 | 510 (0.0012) | 385 | 514 (0.0010) | 384 | 523 (0.0008) | 377 | 505 (0.0001) | 22 141 | 5455 | |
| 6f | 421 | 508 (0.0001) | 432 | 551 (0.0031) | 418 | 575 (0.0041) | 420 | 539 (0.0028) | 398 | 535 (0.0003) | 24 412 | 4999 | |
| 6g | 431 | 494 (0.0002) | 433 | 515 (0.0021) | 414 | 519 (0.0032) | 418 | 507 (0.0011) | 405 | 510 (0.0001) | 39 254 | 3677 | |
| 7 | 438 | 636 (0.0027) | 445 | 615 (0.11) | 424 | 609 (0.087) | 432 | 608 (0.081) | 411 | 592 (0.0031) | 31 424 | 6211 | |

shift ($\lambda_{\text{ex}} \approx 390$ nm and $\lambda_{\text{em}} \approx 500$ nm in DCM) in the optical spectra as conjugation does not permit donor-acceptor interaction (*i.e.*, *meta* linkage). It is important to notice that probe **6d** (R_3 = benzyl substituent) exhibited a relatively higher quantum yield in all solvents when compared to **6b** (R_3 = methyl substituent) which indicated the importance of the substituent (R_3) in the cyanine skeleton with regard to photophysical characteristics.¹² This trend was further consistent with probe series **3** where higher fluorescence quantum yields were exhibited by **3d** (R_3 = benzyl substituent) in comparison to **3a–3c**. One possible explanation for the observed large fluorescence quantum yield in the presence of the benzyl substituent is the relatively high stability and less susceptibility towards photofading of the probe.^{12,33–35}

The attachment of the HBT fragment to the phenyl benzothiazolium (Cy) structure (**6a**) has significantly improved the photophysical properties of the probes **2–5**. Probes **2–5** exhibited significantly high fluorescence quantum yields ($\phi_{\text{fl}} \approx 0.1–0.4$) in comparison with **6**. It is important to notice that probes **2–3** exhibited a significant bathochromic shift in the fluorescence emission ($\lambda_{\text{em}} \approx 600–620$ nm in DCM) due to ESIPT (HBT fragment) coupled with ICT (cyanine fragment) (see Scheme 3). Also, it is important to notice that the absorption spectra of **2–3** did not show a significant bathochromic shift compared to those of probe **6**. This can be explained by considering the connectivity of the HBT moiety to the cyanine fragment *via* the *meta*-phenylene ring system which does not permit the extension of the π -conjugation system of the probe.

3.3 Low temperature fluorescence

The large bathochromic shift observed in the emission of **3** ($\lambda_{\text{em}} \sim 620–640$ nm) in comparison to **6** ($\lambda_{\text{em}} \sim 510–530$ nm) could be attributed to the effect of excited state intramolecular proton transfer (ESIPT) coupled with intramolecular charge transfer (ICT) (Scheme 3). In order to further evaluate the content of the ESIPT effect, we decided to freeze **3b** in liquid nitrogen to limit the molecular motion and bond changes that are associated with the ESIPT process. Thus, the solution of **3b** in a quartz tube was quickly cooled down by immersing the sample into liquid nitrogen in a quartz Dewar and optical



Scheme 3 ESIPT coupling with ICT in HBT-Cy **2–4**.

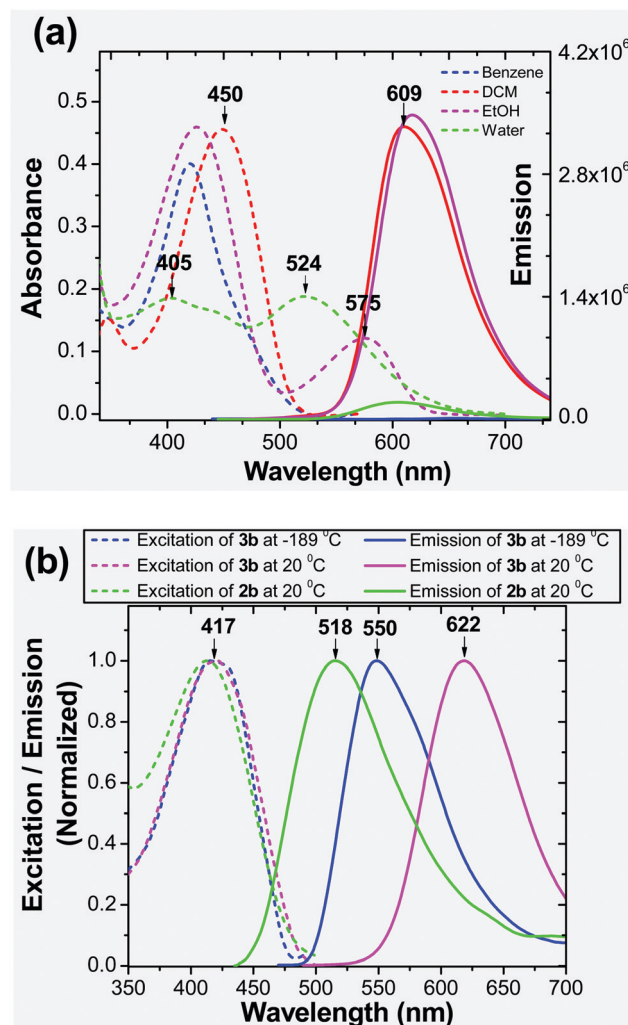


Fig. 1 (a) Absorption and emission of probe **3b** (1×10^{-5} M) in different solvents at room temperature. **3b** was excited at 420 nm. (b) Excitation and emission spectra of **2b** and **3b** (1×10^{-6} M in ethanol) at different temperatures.

spectra were acquired. At an extremely low temperature (at -189 °C), the molecule was frozen in the solvent matrix, which showed the emission peak at about 550 nm (Fig. 1b). When further raising the temperature to room temperature, a bathochromic shift in the emission spectra was observed. The observed spectral shift was quite large $\lambda_{\text{em}} \approx 72$ nm (from 550 nm to ~ 622 nm) in response to the temperature rise. The excitation spectrum of **3b** obtained at -189 °C was nearly identical to that at 20 °C (Fig. 1b), showing the excitation maxima $\lambda_{\text{ex}} = 417$ nm. The observed fluorescence spectral shift at the low temperature was, therefore, related to the rigid molecular environment in the frozen state, which restricts the relaxation of the excited state. In other words, ESIPT and ICT were not fully realized in the frozen solvent matrix, as the bond reorganization and rotation were restricted. The emission spectra of **2b** at room temperature were found to be $\lambda_{\text{em}} \approx 518$ nm which was significantly blue-shifted from the emission spectra of **3b** at -189 °C ($\lambda_{\text{em}} \approx 520$ nm). Since the ESIPT process is entirely

hindered for compound **2b**, the result clearly indicates that the impact of the substituent is $\text{OH} > \text{OCH}_3$. Therefore, the presence of the HBT component in the HBT-Cy skeleton has significantly improved the probe's photophysical properties.

3.4 pH sensitivity

The optical spectra of **3b** were examined in different aqueous pH solutions to evaluate the probe's response (Fig. 2a and ESI,† Fig. S5) under different pH conditions. Probe **3b** was nearly non-fluorescent in basic pH solutions ($\text{pH} > 9$). This can be attributed to the possible deprotonation of the phenolic proton ($\text{Ph-OH} \rightarrow \text{PhO}^- + \text{H}^+$) which eventually hindered ESIPT and resulted in the quenching of fluorescence.^{36,37} Another possible mechanism is the nucleophilic attack (*i.e.*, oxyanion species) that occurs on the cyanine ($\text{C}=\text{N}^+$) bond which disrupts the probe's conjugation and the ICT process. Under basic pH conditions a new peak was observed for **3b** due to the phenoxide formation ($\text{Ph-OH} \rightarrow \text{PhO}^- + \text{H}^+$) in aqueous solution

($\lambda_{\text{max}} = 558 \text{ nm}$). However, probe **3b** become strongly fluorescent in aqueous acidic solutions ($\text{pH} 1\text{--}6$) due to enhanced ESIPT. The calculated pK_a for probe **3b** was found to be 6.01 (ESI,† Fig. S7). It is also imperative to notice that the emission intensities of probe **3b** remain nearly unchanged in the pH range of 4–5 which is close to lysosomal inner pH (≈ 4.5).⁶ According to the calculated pK_a (6.01) for **3b**, the probe will not have significant effect on the pH of the lysosomal lumen (*i.e.*, alkalinizing effect) upon internalization. To further evaluate the role of the phenolic group in pH sensing, **4a** was synthesized as a model compound with two phenolic groups and spectroscopic studies were conducted (Table 1) in comparison to **3b**. In sharp contrast, probe **4a** did not show any significant pH response similar to probe **3b** (ESI,† Fig. S6) under different pH conditions. Also, the emission spectra of **4a** were significantly weaker in all aqueous pH solutions, which was in sharp contrast to **3b**. The calculated average pK_a for **4a** was 6.91 (ESI,† Fig. S7). The observed significant difference in dissociation constants [$K_a(\text{4a})/K_a(\text{3b}) \approx 8$] further explains the decreased acidity of probe **4a**. Therefore, the presence of an additional phenolic group ($\text{R}_4 = \text{OH}$) in **4a** electronically activates the aromatic system which shows that the dissociation of the phenol is partially unfavorable. It is important to notice that the calculated pK_a values for probes **3** and **4** are significantly lower in comparison with basic functional groups such as trialkyl amines ($\text{pK}_a \approx 10.75$) which are often employed in commercial LysoTracker[®] probes. Therefore, HBT-Cy based probes may not exhibit any alkalinizing effect to elevate cellular pH upon internalization. Computational calculations were performed by using the density functional theory method (DFT) by utilizing the B3LYP hybrid function with the 6311G+(2d,p) basis set to calculate the HOMO–LUMO energy levels for probes **3** and **5** under solvent-free, acidic (protonated) and basic (de-protonated) conditions (ESI,† Fig. S25–S27). Probe **3b** exhibited relatively low-lying HOMO energies under all conditions in comparison with **5a**. In addition, the LUMOs of **3b** and **5a** exhibited a higher electron density in the thiazolium fragment (Cy) indicating that strong electronic interaction occurs in the systems involving ICT (ESI,† Fig. S24–S26).

In another experiment, **3b** was dissolved in acidic water ($\text{pH} = 4.5$) and spectroscopically titrated against 10% BSA (in water). A significant fluorescence enhancement ($\approx 200\%$) was observed in **3b** emission upon addition of BSA (Fig. 2b). The pH of the resulting aqueous acidic solution was measured with sequential addition of the BSA to confirm that no significant change in pH occurs during the addition of BSA. The absorption spectra of the probe **3b** showed a significant increase of the peak intensity at $\approx 535 \text{ nm}$ which was attributed to the formation of the phenoxide anion ($\text{Ph-OH} \rightarrow \text{PhO}^-$) (ESI,† Fig. S8). However, it is important to rationalize that the acidic pH environment in the solution ($\text{pH} \approx 4.5$) may not permit the partial deprotonation ($\text{Ph-OH} \rightarrow \text{PhO}^- + \text{H}^+$) of the phenolic group (also see the ESI,† Fig. S5). Therefore, it is possible that **3b** may be internalized into the hydrophobic binding pockets in BSA where partial deprotonation is plausible. Therefore, the observed large fluorescence enhancement could be due to the

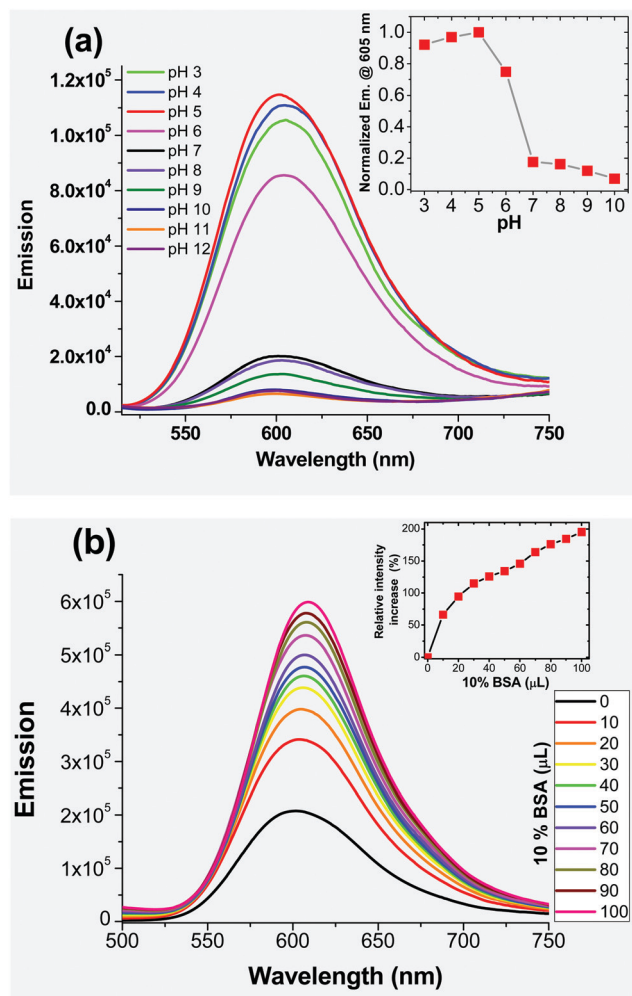


Fig. 2 (a) Emission spectra recorded for probe **3b** ($1 \times 10^{-5} \text{ M}$) in different aqueous pH solutions at room temperature. Probe **3b** was excited at 420 nm. (b) The emission enhancement observed for **3b** ($1 \times 10^{-5} \text{ M}$) in aqueous acidic ($\text{pH} 4.5$) solution upon sequential addition of 10% BSA at room temperature. Probe **3b** was excited at 420 nm.

stabilization of the probe in hydrophobic environments (*i.e.*, the hydrophobic pockets in BSA).^{12,16}

3.5 Biological cell studies

The observed interesting photophysical characteristics led us to investigate the staining ability of probes 2–3 in normal human lung fibroblast (NHLF) and MO3.13 progenitor oligodendrocyte cells. Due to the observed significant fluorescence quantum yield difference in organic and aqueous environments we assumed that probes 2–3 will be possible candidates for cell staining under wash-free conditions.^{11,12,16,38} NHLF cells were initially incubated with probes at a concentration of 500 nM for 30 minutes and visualized by fluorescence confocal microscopy under wash-free conditions (no post staining washing step was carried out prior to imaging). The initial confocal microscopy images obtained for 2–3 showed a non-uniform staining pattern throughout the cell with no noticeable background interference (ESI,† Fig. S9). Further colocalization experiments were performed in the presence of commercial LysoTracker[®] Green DND-26 and LysoTracker[®] Red DND-99 and probes 2–3 showed exceptional colocalization patterns in both NHLF and MO3.13 cell lines (Fig. 3 and ESI,† Fig. S10 and S11). The calculated Mander's overlap coefficient (>0.9 in NHLF in the presence of commercial LysoTracker[®] probes) further confirmed their exceptional selectivity to lysosomes. These results further supported our initial hypothesis that isomeric HBT-Cy versions 2–3 will be excellent markers for cellular lysosome detection similar to previously reported probe 1. In addition, probe 2b ($R_1 = \text{OCH}_3$) produced relatively weak fluorescence images under the 500 nM concentration range and therefore, relatively higher concentrations of 2b (1–2 μM) were used for imaging experiments. This observation can be further explained by considering relatively lower fluorescence quantum yields obtained for 2b (in comparison to 2a). Therefore, the ESIPT enabled HBT-Cy structure (the presence of $-\text{OH}$ instead of $-\text{OCH}_3$) showed significant advantages in fluorescence confocal microscopy. However, it is important to notice that the excellent colocalization images obtained for probe 2b (calculated Mander's overlap coefficient ≈ 0.87) further revealed that the presence of the phenolic group was not mandatory for the “lysosome selectivity” of the probe.

To further investigate the validity of this argument, probes 5a and 5b were synthesized by interchanging fluorophore units across the *meta* phenylene ring of 2a (Scheme 2). Probes 5a and 5b were further studied in NHLF cells in the presence of commercial LysoTracker[®] Green (Fig. 4). Surprisingly, probes 5a ($R_1 = \text{OH}$) and 5b ($R_1 = \text{OCH}_3$) exhibited excellent colocalization (the Mander's overlap coefficient calculated was >0.9) with LysoTracker[®] Green in NHLF cells. Therefore, it was certain that the presence of the phenolic group would enhance the photophysical properties of the probe, however, was not necessary for the lysosome selectivity. Despite the differences in the acidity of the phenolic groups (*i.e.*, 2a vs. 5a), the lysosome selectivity of the probe is independent of the possible phenol/phenoxide ($\text{Ph-OH} \leftrightarrow \text{Ph-O}^- + \text{H}^+$) generation. It is also important to notice that probes 2b and 5b ($R_1 = \text{OCH}_3$) required

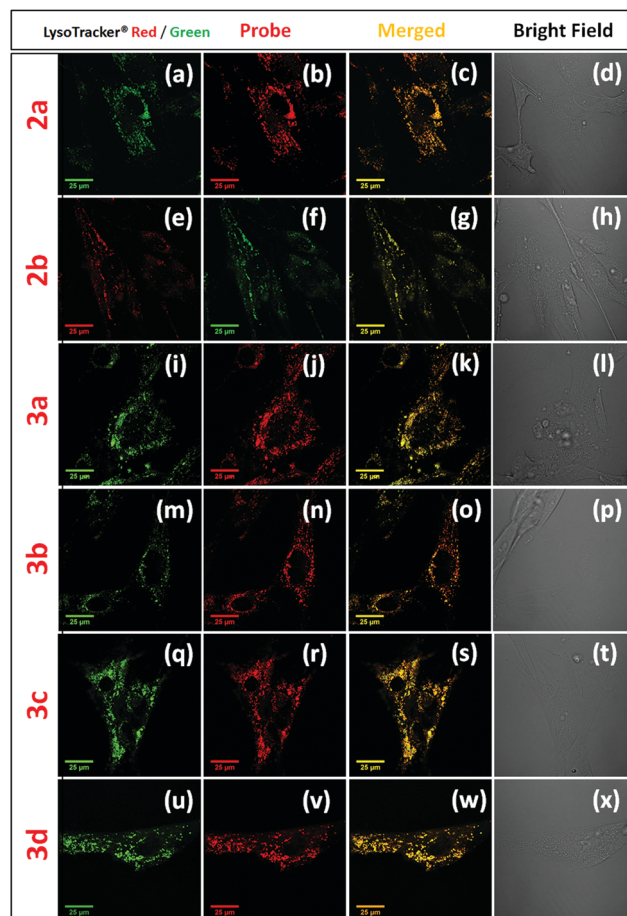


Fig. 3 Fluorescence confocal microscopy images obtained for NHLF cells incubated for 30 minutes with probes 2–3 (500 nM) and LysoTracker[®] Green (70 nM). The probes were excited using a 405 nm laser and LysoTracker[®] Green was excited using a 488 nm laser line. Note: LysoTracker[®] Red (70 nM, 561 nm laser) was used for colocalization of probe 2b. The images from right to left show the staining of the commercial LysoTracker[®], the staining of probes 2–3, the overlapped image, and the bright field image.

post-staining washing steps to minimize background interferences during imaging. Consequently, the employment of the phenolic group in the HBT-Cy probe structure plays an important role in minimizing background fluorescence. In summary, the observed lysosome selectivity in the HBT-Cy probe (2–3) is independent of the connectivity of its fluorophore fragments benzothiazolium cyanine (Cy) and 2-hydroxybenzothiazole (HBT) via a *meta* phenylene ring system. Yet, the ESIPT enables the skeleton (*i.e.*, 2a) to exhibit enhanced photophysical properties (*i.e.*, wash-free staining) in comparison to ESIPT disabled 5a (see Table 1).

To further investigate the effect of the phenolic groups in the HBT-Cy structure on lysosome selectivity we synthesized probe 4a with multiple phenolic components (Scheme 1 and Table 1). Surprisingly, the presence of multiple phenolic groups (*i.e.*, probe 4a where $R_1, R_4 = \text{OH}$) diminish the lysosome selectivity of the probe. The obtained fluorescence confocal microscopy images of 4a in NHLF cells exhibited a bright non-specific staining pattern throughout the entire cell (see Fig. 4(a)–(d)).

However, probe **4a** produced a bright red emission observed by confocal microscopy imaging in NHLF cells with 500 nM concentration for 30 minutes. Therefore, further colocalization images were obtained to investigate the possibility of the selective staining of **4a** under lower concentrations in NHLF cells. However, lowering the **4a** concentration up to 100 nM did not lead to any selective visualization in live cells. However, the presence of multiple phenolic groups improved the fluorescence quantum yield of the probe (see Table 1).

To further investigate the effect of the benzothiazolium component on lysosome selectivity, we synthesized benzothiazolium probes **6a–6g** for studying in biological cells. In biological cell studies, probes **6a–6g** exhibited a good colocalization (Mander's overlap coefficient >0.8–0.7) in the presence of commercial LysoTracker[®] probes (Fig. 5). Nevertheless, the observed colocalization coefficient for probe **6** was noticeably lower than those of probes **2–3** due to the observed significant background fluorescence. This result further revealed that the lysosome selectivity of the probe structure was potentially attributed to the “phenyl benzothiazolium moiety” in the HBT-Cy structure. To further validate this hypothesis and to identify the importance of the benzothiazole fragment with respect to lysosome selectivity, we synthesized and studied **2c** (see Scheme 1 and Table 1) in live cell experiments in the presence of LysoTracker[®] Red (ESI,† Fig. S14). Interestingly **2c** (Schiff base of **2a**) exhibited a remarkable lysosome selectivity confirming the lysosome selectivity arising from the “benzothiazolium (Cy)” fragment and not from the benzothiazole (HBT) component. As a control experiment, probe **7** was synthesized and tested in live cells to investigate its lysosome visualization ability. In sharp contrast, probe **7** did not show any lysosome specificity or internalization into live cells. Therefore, certainly the phenyl benzothiazolium moiety (Cy) in the HBT-Cy structure acts as

the “key component” for the observed lysosome specificity. The fluorescence confocal microscopy images showed a low signal to noise ratio for probe **6** and it is required to stain it with higher probe concentrations (1–2 μM range) with post-staining washing steps to minimize the background interference. However, the fluorescence confocal microscopy imaging results obtained for probe **3** (where the HBT component is connected to probe **6**) showed exceptional lysosome selectivity and excellent photophysical properties. Therefore, the attachment of the 2-hydroxyphenylbenzothiazole (HBT) component to the probe structure significantly enhanced the photophysical properties of the probe to exhibit (1) a large Stokes shift, (2) a high fluorescence quantum yield, (3) red-near infra-red emission, and (4) wash-free application.

The lysosome selectivity of the HBT-Cy probe **3** is independent of the substituent group (R_3) on the cyanine nitrogen atom in the probe structure. These results were further consistent with our previous findings.¹² In addition, the lysosome selectivity of the probes was also independent of the presence of the phenolic group (**2a** vs. **2b**). Due to the positively charged nature of these probes, it is also possible for one to assume that the probes may also show some affinity towards cellular mitochondria where many cationic fluorescent probes have been reported for mitochondrial selectivity.^{10,38,39} Nevertheless, HBT-Cy probes **2**, **3** and **5** did not show any mitochondrial localization in colocalization experiments (ESI,† Fig. S12). Further colocalization experiments were conducted for probe **3** in the presence of commercial ER-Tracker[™] Red (ESI,† Fig. S23) in NHLF cells and the probe did not show any colocalization.

MTT cell proliferation viability assay was performed to investigate the cytotoxicity of probes **2**, **3** and **5** in NHLF cells (ESI,† Fig. S16). The probes exhibited an excellent biocompatibility where the calculated LC_{50} was > 25 μM . In comparison to the working concentration of these probes (*i.e.*, 0.5 μM), the calculated lethal concentration of the probes was significantly higher. Thus, **2**, **3** and **5** will be highly biocompatible and selective fluorescent probes for visualizing cellular lysosomes without perturbing cellular activities. Probe **3d** was further utilized to investigate the possibility of detecting the pH changes in cellular environments. NHLF cells were incubated with different pH buffer solutions (4.5, 7.4 and 10.1) in the presence of probe **3d** (500 nM) and fluorescence confocal microscopy images were obtained (ESI,† Fig. S21). The fluorescence microscopy images were statistically analyzed to investigate their ability to detect pH changes quantitatively. Interestingly, **3d** showed the highest fluorescence emission under physiological pH conditions (pH = 7.4) in comparison to relatively acidic (pH = 4.5) or basic (pH = 10.1) pH conditions. This result indicated the possibility of utilizing probe **3** as a potential fluorescent marker to identify pH fluctuations in biological environments. Probe **3d** was further investigated in NHLF cells to assess its ability to be used as a stable fluorescent marker to visualize cells under stress conditions. NHLF cells were incubated with probe **3d** (500 nM) under normal (cells media + FBS) and stress (cell media with no FBS) conditions for 2 hours and fluorescence microscopy images were obtained (ESI,† Fig. S22). However, probe **3d** did not show

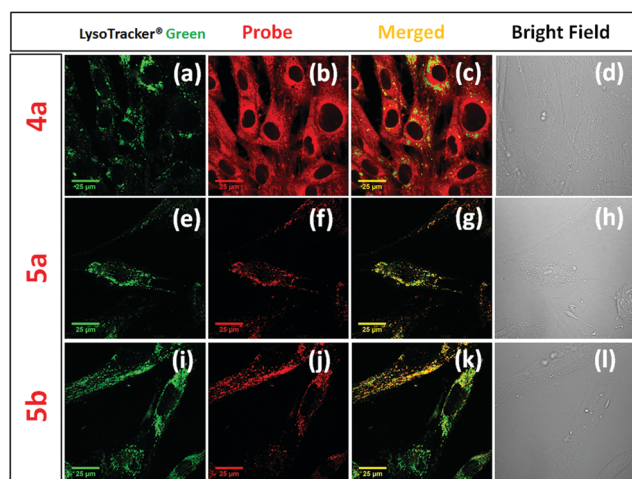


Fig. 4 Fluorescence confocal microscopy images obtained for NHLF cells incubated for 30 minutes with probes **4–5** (500 nM) and LysoTracker[®] Green (70 nm). The probes were excited using a 405/561 nm laser and LysoTracker[®] Green was excited with a 488 nm laser line. The images from right to left show the staining of the commercial LysoTracker[®], staining of probes **4–5**, the overlapped image, and the bright field image.

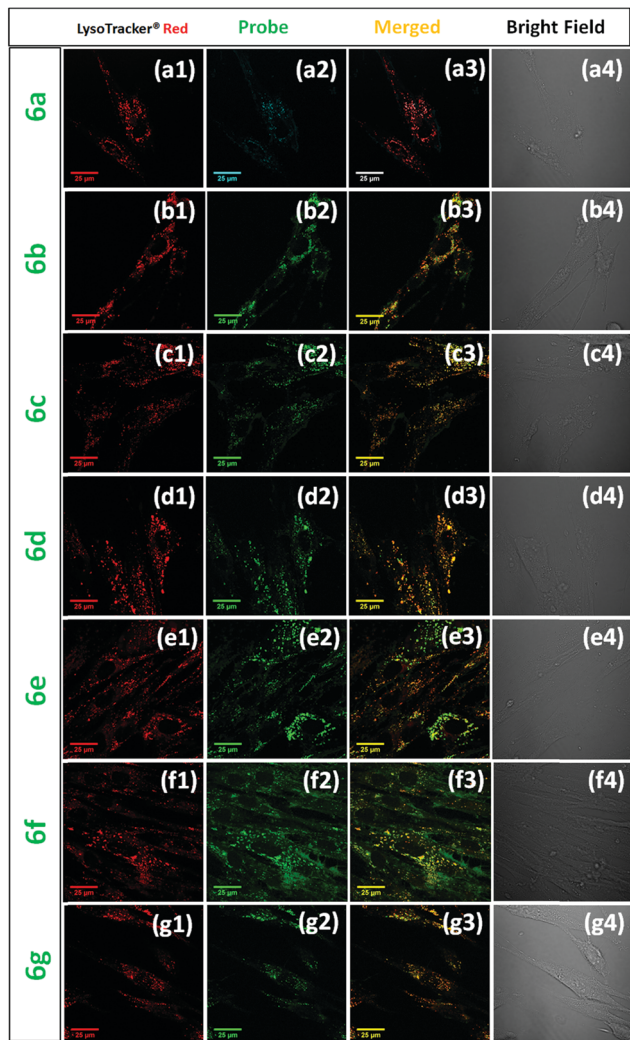


Fig. 5 Fluorescence confocal microscopy images obtained for NHLF cells incubated for 30 minutes with probes **6a–6g** (1 μ M) and LysoTracker[®] Red (70 nm). The probes were excited with a 405 nm laser and LysoTracker[®] Red was excited with a 561 nm laser line. The images from right to left show the staining of the commercial LysoTracker[®], staining of probes **6a–6g**, the overlapped image, and the bright field image.

any noticeable changes in the staining pattern or the calculated fluorescence intensity which indicates its possibility to stain cellular lysosomes under different stress conditions. To further evaluate the probe's intrinsic properties to stain cellular lysosomes under different stress conditions and fluctuations, NHLF cells were initially incubated with 1 μ M carbonyl cyanide-*p*-trifluoromethoxyphenylhydrazone (FCCP) for 1 hour. Then the cells were further incubated with probe **3d** for 30 minutes and analyzed *via* fluorescence confocal microscopy. FCCP acts as a mitochondrial membrane potential inhibitor which disrupts ATP synthesis by acting as an uncoupler. Interestingly, probe **3d** generated excellent confocal microscopy images in the presence of FCCP which further confirms the ability of probe **3** to be used as a potential fluorescent marker to detect cellular lysosomes under different stress conditions (ESI,† Fig. S23). The probe's lysosome selectivity under stress

conditions was further confirmed by performing colocalization experiments in the presence of LysoTracker[®] Green DND-26 (ESI,† Fig. S24).

3.6 Long-term imaging ability and photostability evaluation

Probes **2–3** were identified as the most promising lysosome selective fluorescent probes in the reported series. Further experiments were performed to evaluate the long-term imaging ability and the photostability of the probes. NHLF cells were incubated with probe **3d** (500 nM) for 30 minutes and fluorescence confocal microscopy images were analyzed in 30 minute time intervals up to 4 hours (Fig. 6a and ESI,† Fig. S18). Interestingly, probe **3d** generated stable localization patterns within the cell up to 4 hours without generating any noticeable background interferences or morphological changes. The normalized fluorescence intensity of the probe **3d** emission in live cells was plotted as a function of imaging time (Fig. 6b). These results further illustrated the inherent biocompatibility and high photostability of the probe in biological environments though the probe is excitable with a relatively high energy (405 nm) laser line. To further investigate the photostability and possible phototoxicity of these probes, NHLF cells were

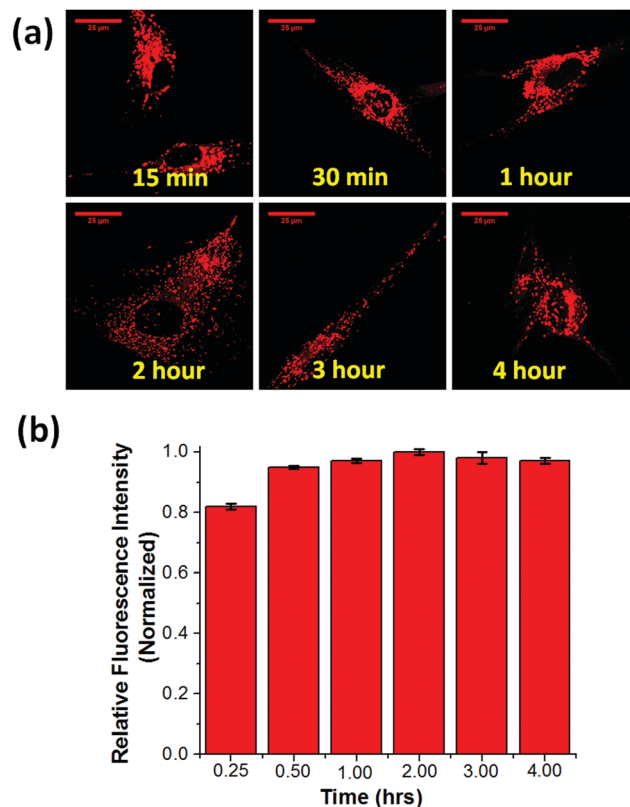


Fig. 6 (a) Long-term imaging ability assessment for probe **3d** in NHLF cells. The cells were incubated with **3d** (500 nM) for 30 minutes and confocal microscopy images were obtained at different time intervals under consistent parameters of the microscope. Probe **3d** was excited using a 405 nm laser and the emissions were collected in the 570 nm to 700 nm range. (b) The averaged normalized fluorescence intensity obtained for probe **3d** at different time intervals.

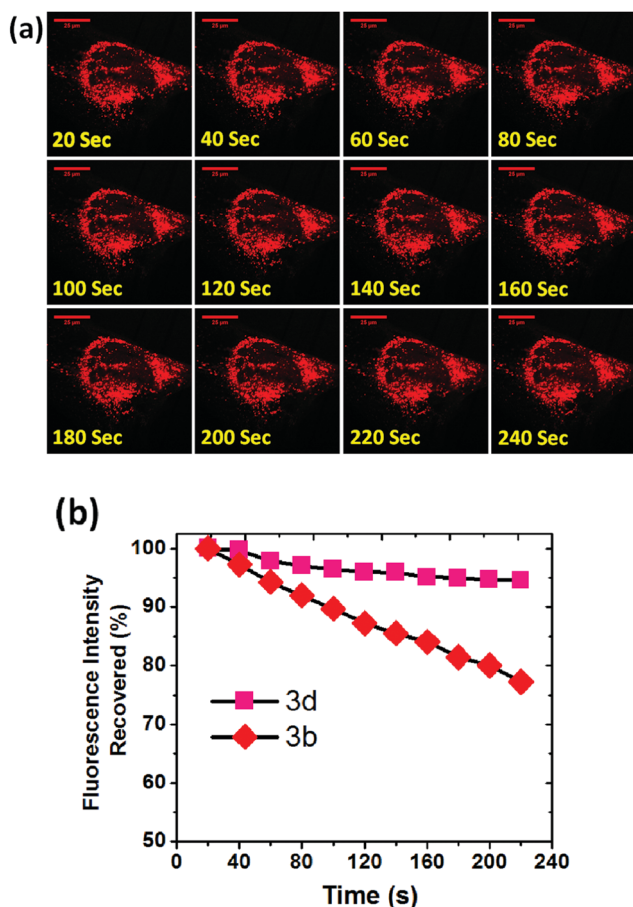


Fig. 7 (a) Fluorescence confocal microscopy images obtained for probe **3d** (500 nM) in NHLF cells upon continuous irradiation with a 405 nm laser line (laser power percentage 3.0; digital zoom = 1; pinhole = 1AU; master gain = 150; digital offset = 0). Fluorescence confocal microscopy images were obtained at 20 s time intervals. (b) The plot of recovered fluorescence intensity versus irradiation time calculated for **3b** (500 nM) and **3d** (500 nM).

incubated with **3b** and **3d** (500 nM) for 30 minutes and continuous irradiation was obtained using a 405 nm laser for 4 minutes. Fluorescence confocal microscopy images were obtained at 20 s time intervals during the experiment (Fig. 7 and ESI,† Fig. S19, S20). The recovered fluorescence intensity (%) was plotted as a function of irradiation time (Fig. 7b). The recovered fluorescence intensity analysis further revealed that the possible photobleaching of the probe upon continuous irradiation is minimal under experimental conditions. Therefore, these probes will be reliable candidates for imaging cellular lysosomes *via* fluorescence confocal microscopy. However, it is also important to notice that probe **3d** exhibited relatively more stability towards photobleaching in comparison to **3b**. This result also suggested that the substituent on the benzothiazolium segment had a large impact on the photostability of the probe.¹² The observed relatively lower photostability of **3b** was due to the possible photodegradation of the probe upon interaction with molecular oxygen singlet oxygen ($^1\text{O}_2$) or the superoxide anion (O_2^-) present in the biological environments.^{33,34} These results further suggested that the relative electron density on the cyanine N atom can affect its photostability.^{12,34}

4. Conclusions

In summary, a series of HBT-Cy fluorescent probes were synthesized in high yields. HBT-Cy probes **2a** and **3** exhibited excellent fluorescence quantum yields ($\phi_{\text{fl}} \approx 0.1\text{--}0.5$) and a large Stokes shift ($\Delta\lambda > 130$ nm) due to excited state intramolecular proton transfer coupled with intramolecular charge transfer. Compared to the simple benzothiazolium version (Cy) **6**, probes **2–3** exhibited excellent photophysical characteristics due to the attachment of the 2-(2'-hydroxyphenyl)benzothiazole (HBT) fragment to the benzothiazolium (Cy) moiety. The substituent on the cyanine nitrogen atom (R_3) affected the fluorescence quantum yield of the compounds and higher fluorescence quantum yields were obtained for probes with bulky groups ($\text{R}_3 = \text{PhCH}_2$) on cyanine nitrogen. The low temperature results proved that the HBT group plays an important role in the large Stokes shift due to ES IPT. Probe **3** exhibited significant sensitivity towards pH changes in aqueous solutions. Thus, the calculated pK_{a} values ($\text{pK}_{\text{a}} < 7$) further confirmed the non-alkalinizing properties of the probes. Probes **2**, **3** and **5** showed excellent lysosome selectivity in live cell imaging. The lysosome selectivity of probes **2–3** was independent of the (1) substituent (R_3) on the cyanine nitrogen atom, (2) connectivity order of the cyanine and HBT fragments *via* the *meta* phenylene ring, and (3) presence/absence of the phenolic group. However, the attachment of a single phenolic group significantly improved the photophysical properties of the probe (*i.e.*, **2a** vs. **2b**). The attachment of multiple phenolic groups in the probe structure diminished the lysosome selectivity of the probe (*i.e.*, probe **4a**). The experimental results indicated that the phenyl benzothiazolium (Cy) moiety **6** is the key component for the observed lysosome selectivity. Probes **2a**, **3**, and **5a** produced excellent fluorescence confocal images of the cellular lysosomes under wash-free conditions with a high signal to noise ratio. Probes **2**, **3** and **5** exhibited high biocompatibility ($\text{LC}_{50} > 25 \mu\text{M}$) for live cell applications. Probe **3** exhibited excellent photostability and long-term imaging ability during the fluorescence confocal microscopy. In addition probe **3** was successfully utilized to visualize cellular lysosomes under different stress conditions. The attachment of the 2-hydroxyphenylbenzothiazole (HBT) fragment to the probe structure significantly enhanced the photophysical characteristics of the probes (**2–3**) including (1) wash free application, (2) bright fluorescence, (3) high stability, (4) large Stokes shift, (5) high photostability and (6) high biocompatibility. The HBT skeleton **7** did not exhibit any lysosome specificity in the absence of the benzothiazolium (Cy) component. Therefore, this new HBT-Cy based lysosome probe design would be a superior replacement for existing commercial LysoTracker[®] probes for cellular applications under non-alkalinizing conditions.

Author contributions

C. S. A. planned, conducted, and summarized the synthesis and characterization of probes. C. S. A., K. A. B. and L. J. M. planned and performed cell imaging experiments. C. S. A. and D. D.

performed the photophysical characterization of the probes. N. A. conducted and summarized the mass spectra for the probes. H. J. B. conducted the cell viability experiments. C. R. S. performed computational calculations. Y. P. supervised the project. C. S. A and Y. P. wrote the manuscript.

Conflicts of interest

There are no conflicts to declare.

Acknowledgements

The NHLF cell line was a kind gift from Dr Sailaja Parachuri at the University of Akron. We thank Dr Leah Shriver at the University of Akron for providing the MO.3.13 cell line and cell culture facility. We also thank Prof. Robert Stahelin (Purdue University) and Dr Kaveesha Wijesinghe (University of Notre Dame) for valuable discussions and guidance.

References

- C. de Duve and R. Wattiaux, *Annu. Rev. Physiol.*, 1966, **28**, 435–492.
- S. Piao and R. K. Amaravadi, *Ann. N. Y. Acad. Sci.*, 2016, **1371**, 45–54.
- B. Alberts, D. Bray, K. Hopkin, A. Johnson, J. Lewis, M. Raff, K. Roberts and P. Walter, *Essential cell biology*, Garland Science, 2013.
- J. P. Luzio, Y. Hackmann, N. M. G. Dieckmann and G. M. Griffiths, *Cold Spring Harbor Perspect. Biol.*, 2014, **6**(9), a016840.
- U. Repnik, V. Stoka, V. Turk and B. Turk, *Biochim. Biophys. Acta, Proteins Proteomics*, 1824, **2012**, 22–33.
- J. P. Luzio, P. R. Pryor and N. A. Bright, *Nat. Rev. Mol. Cell Biol.*, 2007, **8**, 622.
- A. Thorburn, D. H. Thamm and D. L. Gustafson, *Mol. Pharmacol.*, 2014, **85**, 830–838.
- T. Kirkegaard and M. Jäättelä, *Biochim. Biophys. Acta, Mol. Cell Res.*, 1793, **2009**, 746–754.
- N. Fehrenbacher, N. Fehrenbacher, M. Jäättelä and M. Jäättelä, *Cancer Res.*, 2005, **65**, 2993–2995.
- G. Y. Wiederschain, *Biochemistry*, 2011, **76**, 1276.
- D. Dahal, L. McDonald, X. Bi, C. Abeywickrama, F. Gombedza, M. Konopka, S. Paruchuri and Y. Pang, *Chem. Commun.*, 2017, **53**, 3697–3700.
- C. S. Abeywickrama, K. J. Wijesinghe, R. V. Stahelin and Y. Pang, *Chem. Commun.*, 2019, **55**(24), 3469–3472.
- B. Wang, S. Yu, X. Chai, T. Li, Q. Wu and T. Wang, *Chem. – Eur. J.*, 2016, **22**, 5649–5656.
- X. Zhang, C. Wang, Z. Han and Y. Xiao, *ACS Appl. Mater. Interfaces*, 2014, **6**, 21669–21676.
- N. B. Yapici, Y. Bi, P. Li, X. Chen, X. Yan, S. R. Mandalapu, M. Faucett, S. Jockusch, J. Ju, K. M. Gibson, W. J. Pavan and L. Bi, *Sci. Rep.*, 2015, **5**, 8576.
- K. A. Bertman, C. S. Abeywickrama, H. J. Baumann, N. Alexander, L. McDonald, L. P. Shriver, M. Konopka and Y. Pang, *J. Mater. Chem. B*, 2018, **6**, 5050–5058.
- J. P. Luzio, B. A. Rous, N. A. Bright, P. R. Pryor, B. M. Mullock and R. C. Piper, *J. Cell Sci.*, 2000, **113**(Pt 9), 1515–1524.
- R. G. W. Anderson and L. Orci, *J. Cell Biol.*, 1988, **106**, 539–543.
- W. Zhu, X. Zheng, Y. Huang, Z. Lu and H. Ai, *Sci. China: Chem.*, 2018, 1–7.
- R. P. Haugland, *The handbook: a guide to fluorescent probes and labeling technologies*, Molecular probes, 2005.
- M. Fang, R. Adhikari, J. Bi, W. Mazi, N. Dorh, J. Wang, N. Conner, J. Ainsley, T. G. Karabancheva-Christova, F.-T. Luo, A. Tiwari and H. Liu, *J. Mater. Chem. B*, 2017, **5**, 9579–9590.
- Y. Han, M. Li, F. Qiu, M. Zhang and Y.-H. Zhang, *Nat. Commun.*, 2017, **8**, 1307.
- K. A. Bertman, C. S. Abeywickrama, A. Ingle, L. P. Shriver, M. Konopka and Y. Pang, *J. Fluoresc.*, 2019, 1–9.
- J. Ou-Yang, W.-L. Jiang, K.-Y. Tan, H.-W. Liu, S.-J. Li, J. Liu, Y.-F. Li and C.-Y. Li, *Sens. Actuators, B*, 2018, **260**, 264–273.
- J. Ou-Yang, Y.-F. Li, P. Wu, W.-L. Jiang, H.-W. Liu and C.-Y. Li, *ACS Sens.*, 2018, **3**, 1354–1361.
- X. Zhang, B. Wang, C. Wang, L. Chen and Y. Xiao, *Anal. Chem.*, 2015, **87**, 8292–8300.
- Q. Wan, S. Chen, W. Shi, L. Li and H. Ma, *Angew. Chem., Int. Ed.*, 2014, **53**, 10916–10920.
- H. Lim, H. Park and H. P. Kim, *Biochem. Pharmacol.*, 2015, **96**, 337–348.
- L. Groth-Pedersen and M. Jäättelä, *Cancer Lett.*, 2013, **332**, 265–274.
- G. Kroemer and M. Jäättelä, *Nat. Rev. Cancer*, 2005, **5**, 886.
- P. Jiang and N. Mizushima, *Cell Res.*, 2014, **24**, 69–79.
- A. Pierzyńska-Mach, P. A. Janowski and J. W. Dobrucki, *Cytometry, Part A*, 2014, **85**, 729–737.
- C. Chen, B. Zhou, D. Lu and G. Xu, *J. Photochem. Photobiol., A*, 1995, **89**, 25–29.
- X. Chen, X. Peng, A. Cui, B. Wang, L. Wang and R. Zhang, *J. Photochem. Photobiol., A*, 2006, **181**, 79–85.
- S. J. Formosinho and L. G. Arnaut, *J. Photochem. Photobiol., A*, 1993, **75**, 21–48.
- C. S. Abeywickrama and Y. Pang, *Tetrahedron Lett.*, 2017, **58**, 1627–1632.
- C. S. Abeywickrama and Y. Pang, *Tetrahedron Lett.*, 2016, **57**, 3518–3522.
- C. S. Abeywickrama, K. J. Wijesinghe, R. V. Stahelin and Y. Pang, *Sens. Actuators, B*, 2019, **285**, 76–83.
- C. S. Abeywickrama, H. J. Baumann, N. Alexander, L. P. Shriver, M. Konopka and Y. Pang, *Org. Biomol. Chem.*, 2018, **16**, 3382–3388.